

Metabolic Reprogramming by Dual AKT/ERK Inhibition through Imipridones Elicits Unique Vulnerabilities in Glioblastoma



Chiaki T. Ishida¹, Yiru Zhang¹, Elena Bianchetti¹, Chang Shu¹, Trang T.T. Nguyen¹, Giulio Kleiner², Maria J. Sanchez-Quintero², Catarina M. Quinzii², Mike-Andrew Westhoff³, Georg Karpel-Massler⁴, Varun V. Prabhu⁵, Joshua E. Allen⁵, and Markus D. Siegelin¹

Abstract

Purpose: The goal of this study is to enhance the efficacy of imipridones, a novel class of AKT/ERK inhibitors that displayed limited therapeutic efficacy against glioblastoma (GBM).

Experimental Design: Gene set enrichment, LC/MS, and extracellular flux analyses were used to determine the mechanism of action of novel imipridone compounds, ONC206 and ONC212. Orthotopic patient-derived xenografts were utilized to evaluate therapeutic potency.

Results: Imipridones reduce the proliferation of patient-derived xenograft and stem-like glioblastoma cell cultures *in vitro* and in multiple xenograft models *in vivo*. ONC212 displayed the highest potency. High levels of c-myc predict susceptibility to growth inhibition and apoptosis induction by imipridones and increased host survival in orthotopic patient-derived xenografts. As early as 1 hour, imipridones elicit on-target inhibition, followed by dephosphorylation of GSK3 β at serine 9. GSK3 β promotes phosphorylation

of c-myc at threonine 58 and enhances its proteasomal degradation. Moreover, inhibition of c-myc by BRD4 antagonists sensitizes for imipridone-induced apoptosis in stem-like GBM cells *in vitro* and *in vivo*. Imipridones affect energy metabolism by suppressing both glycolysis and oxidative phosphorylation, which is accompanied by a compensatory activation of the serine-one carbon-glycine (SOG) pathway, involving the transcription factor ATF4. Interference with the SOG pathway through novel inhibitors of PHGDH results in synergistic cell death induction *in vitro* and *in vivo*.

Conclusions: These results suggest that c-myc expression predicts therapeutic responses to imipridones and that imipridones lead to suppression of tumor cell energy metabolism, eliciting unique metabolic vulnerabilities that can be exploited for clinical relevant drug combination therapies. *Clin Cancer Res*; 24(21); 5392–406. ©2018 AACR.

Introduction

Imipridone derivatives are a new class of molecules that have entered clinical testing for solid and nonsolid malignancies. Representative examples are the lead compound, called ONC201 (1), and the chemically modified and presumably enhanced derivatives, ONC206 and ONC212 (2). The original compound, ONC201, was identified in a screen for molecules that induce TRAIL, a cytokine that in the field of oncology was considered as the holy grail for cancer therapy because it specifically kills tumor cells in a rapid manner, but not nonneoplastic cells (1). On the molecular level, ONC201 elicited an increase of TRAIL transcription through a FOXO3A-dependent mechanism, involving the

inhibition of the kinases ERK and AKT (1). Early after the discovery of ONC201, it became evident that this compound exerts additional anticancer properties, e.g., the inhibition of proliferation in cells that do not undergo apoptosis upon ONC201 administration (3–5). These additional features are in part attributed to the fact that imipridones inhibit dopamine receptor signaling, such as DRD2 (6).

Tumor cell metabolism has become a central focus in cancer research because it bears the potential to target metabolic aberrancies in tumors, thus providing a therapeutic window. Although cancer cells often depend on glycolysis in the presence of abundant oxygen (called Warburg effect), it has become evident that other metabolic pathways are targetable in malignant cells, even oxidative phosphorylation (OXPHOS), the most efficient form of energy generation in cells. Quite prominent is the metabolic dependency on glutamine by many malignant tumors (7–9), which requires the presence of a functional OXPHOS. Being a master regulator of tumor stem cells, the transcription factor c-myc (10–12) is at the core of regulation of tumor cell metabolism and affects the expression of enzymes related to glycolysis, glutamine, and OXPHOS.

In this report, we provide evidence that novel imipridones with different potency are highly effective against state-of-the-art model systems of glioblastoma, involving in particular glioma stem-like cells. We have unraveled a novel mechanism by which imipridones elicit their anti-glioma activity, involving suppression of the master regulator, c-myc, as early as 1 hour, and shut down of

¹Department of Pathology and Cell Biology, Columbia University Medical Center, New York, New York. ²Department of Neurology, Columbia University Medical Center, New York, New York. ³Department of Pediatrics and Adolescent Medicine, Ulm University Medical Center, Ulm, Germany. ⁴Department of Neurosurgery, Ulm University Medical Center, Ulm, Germany. ⁵Oncoceutics, Inc., Philadelphia, Pennsylvania.

Note: Supplementary data for this article are available at Clinical Cancer Research Online (<http://clincancerres.aacrjournals.org/>).

Corresponding Author: Markus D. Siegelin, Columbia University Medical Center, 630 West, 168th Street, P&S Rm. 15-401, New York, NY 10032. Phone: 212-305-1993; E-mail: ms4169@cumc.columbia.edu

doi: 10.1158/1078-0432.CCR-18-1040

©2018 American Association for Cancer Research.

Translational Relevance

Imipridones have recently entered clinical testing for hematologic and solid malignancies, including glioblastoma, the most common primary brain tumor that requires novel treatments. In the current study, we provide evidence that chemically modified imipridones, ONC206 and ONC212, exert more potent antiglioma activity than the original lead compound, ONC201. Moreover, we demonstrate that high levels of c-myc predict therapeutic responses in preclinical model systems of glioblastoma. Notably, single treatment of ONC212 significantly extends host survival in an orthotopic patient-derived glioblastoma xenograft model. Combined treatment with a clinically validated BRD4 antagonist, OTX015, and imipridones induces enhanced reduction of glioma growth *in vitro* and *in vivo*. These observations support the notion that chemically modified imipridones display preclinical activity singly or as part of combination therapies in model systems of glioblastoma. Therefore, clinical testing of these novel compounds either singly or in combination therapies is warranted.

tumor energy cell metabolism, leading to a state of energy deprivation and tumor cell cytoskeleton and apoptosis. Moreover, high levels of c-myc predict both apoptotic response and inhibition of proliferation of GBM cells to imipridone derivatives and extended host survival in orthotopic patient-derived xenografts (PDX) of glioblastoma, positioning c-myc as a potential therapeutic predictive marker, and that further inhibition of c-myc along with imipridones induces synergistic growth reduction *in vitro* and *in vivo*. In addition, we have unraveled that upon imipridone-induced energy deprivation, the serine-one carbon-glycine pathway is increased, eliciting a novel unique metabolic vulnerability.

Materials and Methods

Reagents

Imipridones, ONC201, ONC206, and ONC212, were received from Oncoceutics. OTX015 was purchased from Selleckchem. A 10 mmol/L working solution in dimethylsulfoxide (DMSO) was prepared for all reagents prior to storage at -20°C . Final concentrations of DMSO were below 0.1% (v/v). The plasmids for wild-type c-myc and mutant c-myc were obtained from Addgene (ID: 45597 and 45598).

Cell cultures and growth conditions

All cells were cultured as described (13–17). The identities of the cell cultures were confirmed by the respective source of purchase. LN229 and U87 cells are established glioblastoma cells. SF188 is an MYC-amplified pediatric glioblastoma cell culture. NCH644, NCH690, and NCH421K glioma stem-like cells were cultured in MG-43 medium (CLS) for both maintenance and experiments (13–15, 18). GBM12 and GBM14 are PDX tumors as described elsewhere (13–17). Human astrocytes were obtained from ScienCell Research Laboratories, Inc. and cultured as recommended by the provider.

Cell viability assays

In order to examine cellular proliferation, CellTiter-Glo assays were performed as previously described. ATP levels were determined as performed in refs. 13–17.

Measurement of apoptosis and mitochondrial membrane potential

Annexin V/propidium iodide, propidium iodide, and tetramethylrhodamine, ethyl ester (TMRE) staining (for mitochondrial membrane potential) were performed as previously described (13–17) or in accordance with the manufacturer instructions for TMRE staining (Cell Signaling Technology). The data were analyzed with the FlowJo software (version 8.7.1; Tree Star).

Extracellular flux analysis

Extracellular flux analysis was performed on the Seahorse XFe24 Analyzer. The "XF cell mito stress test kit" (Agilent Technologies) was utilized to determine parameters relevant to oxidative phosphorylation and determined as described earlier in ref. 19. GBM cells were incubated with Seahorse XF base medium supplemented with 5 mmol/L glucose, 1 mmol/L pyruvate, and 2 mmol/L L-glutamine in a CO_2 -free incubator for 1 hour before the assay. During the course of the assay, 2 $\mu\text{mol/L}$ oligomycin, 2 $\mu\text{mol/L}$ FCCP, and 0.5 $\mu\text{mol/L}$ rotenone/antimycin were added sequentially. Regarding glycolysis, the "XF cell glycolysis stress test kit" (Agilent Technologies) was used in accordance with manufacturer's instructions. GBM cells were incubated with Seahorse XF base medium supplemented with 1 mmol/L L-glutamine in a CO_2 -free incubator for 1 hour before the assay. During the course of the assay, 10 mmol/L glucose, 1 $\mu\text{mol/L}$ oligomycin, and 50 mmol/L 2-DG were added sequentially.

LC/MS analysis of metabolites

Metabolite analysis was carried out on a Thermo Scientific QExactive Orbitrap in a manner as described earlier by others (20).

Western blot analysis and capillary electrophoresis on Wes instrument (Proteinsimple)

Specific protein expression in cell lines was determined by Western blot analysis or capillary electrophoresis as described before. Capillary electrophoresis was run on the Wes instrument (Proteinsimple). The following antibodies were used on the Wes instrument: p-Akt (serine 473; 1:25; CST, Cell Signaling Technology), Akt (1:50; CST), Mcl-1 (1:50; CST), Bcl-2 (1:25; R&D Systems), BIM (1:25; CST), Bcl-xL (1:25; CST), c-myc (1:25; CST), Usp9X (1:25; CST), Noxa (1:25, clone 114C307; Calbiochem), p-Akt (1:25; CST), Akt (1:25; CST), p-AMPK (1:25; CST), AMPK (1:25; CST), PHGDH antibody (Novus; #NBP1-87311), PSAT1 Polyclonal Antibody (Invitrogen; #PA5-22124), β -actin (1:250, clone AC15; Sigma Aldrich), and secondary horseradish peroxidase-linked antibodies were purchased from Santa Cruz Biotechnology Inc. For the expression levels of respiratory complexes, the Total OXPHOS Human WB Antibody Cocktail was used (Abcam). Western blots were acquired, using the Azure (C300) imaging system (CCD – camera based).

Real-time PCR analysis

RNA was isolated and reverse-transcribed as previously described (21). For cDNA amplification, c-myc primers were used: Forward: CCT GGT GCT CCA TGA GGA GAC; Reverse: CAG ACT CTG ACC TTT TGC GAG G. Amplification of 18S served as normalization control. For the determination of mtDNA, the following primers were used: Forward cga aag gac aag aga aat aag g; Reverse: ctg taa agt ttt aag ttt tat gcg. The other primers were designed by Origene Technologies.

Ishida et al.

Microarray and gene set enrichment analysis

Transcriptome analysis and gene set enrichment analysis (GSEA), involving microarrays, were performed as previously described in ref. 21. The related data and cel files are archived through GEO under the following accession numbers: GSE104273 and GSE103963.

Transfections of siRNAs or transductions of shRNAs

Transfections were performed as previously described (22), using either Oligofectamine or Lipofectamine 2000. CMYC siRNA 1 and 2 were purchased from Cell Signaling Technology. DRD2-specific siRNAs were obtained from Dharmacon. Non-targeting siRNA-pool (ON-TARGETplus Non-targeting Pool, # D-001810-10-20) was purchased from Dharmacon. Lentiviral shRNA particles targeting c-myc were purchased from Santa Cruz Biotechnology.

Orthotopic xenograft models of glioblastoma

The individual cells were injected as previously described in refs. 16, 21. Briefly, 50,000 U87 cells or 3×10^5 GBM123 cells in 2 μ L of PBS were intracranially injected into nu/nu mouse. After 3 days of engraftment, the drug treatments were initiated. All treatments were administered by i.p. injection.

Subcutaneous xenograft model

NCH644 (GBM stem-like cells), U87-EGFRvIII, or HCT116 (colon carcinoma) cells were suspended 1:1 in Matrigel Matrix (Corning Inc.) and implanted subcutaneously into the flanks of 6- to 8-week-old Nu/Nu mice. Tumors were measured with a caliper and sizes calculated according to the standard formula: $(\text{length} \times \text{width}^2) \times 0.5$. All treatments were administered by i.p. injection. Drug compounds were dissolved in 10% DMSO, 32% Cremophor EL (SIGMA), 8% Ethanol (Pharmco-Aaper), and 50% PBS.

Immunohistochemistry

PDX xenografted tumors were fixed in formalin and embedded in paraffin as previously described (13). Paraffin sections were cut and stained with hematoxylin and eosin or subjected to immunohistochemistry for TUNEL or Ki67 staining as described (13).

Statistical analysis

Statistical significance was assessed by two-tailed Student *t* test or the Mann-Whitney test using Prism version 5.04 (GraphPad). A $P \leq 0.05$ was considered statistically significant.

Study approval

All procedures were in accordance with Animal Welfare Regulations and approved by the Institutional Animal Care and Use Committee at the Columbia University Medical Center.

Results

High levels of c-myc protein predict apoptosis induction and inhibition of proliferation by imipridones in model systems of GBM

The chemical structures of the different imipridones are shown in Fig. 1A. Therein, ONC201 represents the lead compound, whereas ONC206 and ONC212 are chemically modified derivatives with anticipated enhanced efficacy (Fig. 1A). To get an understanding of the underlying cause of the observed reduction

in cellular viability, we conducted cell-cycle analysis of GBM cultures after treatment with various imipridones for 72 hours. Our observations suggested that GBM cells with high c-myc levels were more likely to respond with apoptosis induction upon imipridone (ONC201, ONC206, and ONC212) treatment (Fig. 1B–G; Supplementary Fig. S1F). While in PDX GBM14 cells, established LN229, T98G and U87 GBM (lower levels) cells we only observed a settle increase in sub-G1 (apoptotic) cells (Fig. 1B and C), this effect was more pronounced in stem-like NCH644, NCH690, and NCH421k cells as well as in a pediatric GBM cell line, SF188 (all very high c-myc expression; Supplementary Fig. S1; Fig. 1B and E–G). Consistent with the highest expression levels of c-myc, NCH421k glioma stem-like cells underwent apoptosis most strikingly upon administration of imipridones (Fig. 1B, E, and G; Supplementary Fig. S1C). Similarly, NCH690 glioma stem-like cells treated with various imipridones displayed a high fraction of Annexin V–positive cells (Supplementary Fig. S1B and S1D), which occurred in a time-dependent manner (Supplementary Fig. S1A–S1C). Notably, c-myc suppression precedes apoptosis induction in NCH421k cells (Supplementary Fig. S1A–S1C). Among imipridones, ONC212 (nanomolar range) was most potent to elucidate these changes when compared with ONC201 (micromolar range; Fig. 1B and G; Supplementary Fig. S1). However, despite the fact that intermediate c-myc–expressing cells (U87) or low c-myc–expressing cells (GBM14) did not undergo apoptosis, they still display inhibition of proliferation (IC_{50} values) upon imipridone administration in accordance with their expression level of c-myc (Fig. 1E and G). Notably, nonneoplastic human astrocytes displayed the highest resistance against imipridones (Fig. 1G).

We modulated the expression levels of c-myc in an intermediate expressing c-myc line, U87, as well as in MYC-amplified SF188 cells (very high levels). We confirmed that SF188 cells are acutely dependent on c-myc for their survival. To test this hypothesis, we acutely silenced the expression of c-myc by two c-myc targeting siRNAs and subsequently analyzed them for apoptosis induction (Supplementary Fig. S1E). Our findings indicate that silencing of c-myc elicited significant apoptosis induction in these cells, reinforcing their dependence on the transcription factor, c-myc. Next, we created a stable cell c-myc–overexpressing U87 line and evaluated its susceptibility to ONC201 in the context of apoptosis induction (Fig. 1H and I). In agreement with our hypothesis, we found that c-myc–overexpressing cells displayed a higher rate of DNA fragmentation upon imipridone treatment as compared with control-transduced cells. In a reciprocal approach, we created a stable SF188 line with silenced c-myc expression (lentiviral shRNA) that in turn becomes less addicted to c-myc. As anticipated, SF188 GBM cells with silenced c-myc expression were less sensitive to apoptosis induction by imipridones as compared with cells transduced with a nontargeting shRNA (Fig. 1J and K). These findings suggest that imipridones mediate their effects in part by inhibition of proliferation and apoptosis induction in a cell-type and c-myc–dependent manner.

Imipridones regulate phosphorylation of AKT, ERK, and FOXO3A, mTORC1 signaling, expression of anti- and proapoptotic Bcl-2 family members, and c-myc protein levels in GBM model systems

To assess the pharmacodynamics properties of imipridones in model systems of GBM, we performed protein capillary electrophoresis for the expression of phosphorylated Akt, total Akt,

phosphorylated ERK, total ERK, phosphorylated FOXO3A (downstream targets of AKT and ERK), and total FOXO3A in U87 and stem-like GBM cell, NCH644, after treatment with ONC201, ONC206, and ONC212 at 200 nmol/L for 72 hours (Fig. 2A; Supplementary Fig. S2A). Although, as anticipated, ONC201 did not show activity, ONC212 was most potent to affect the phosphorylation status of FOXO3A, Akt, and ERK, in keeping with the cellular viability assays. However, higher concentrations of ONC201 resembled the above findings related to ONC212. Next, we assessed the activation status of mTORC1 signaling after imipridone exposure to U87 and stem-like GBM cell, NCH644, because earlier findings suggested that ONC201/TIC10 interfered with this signaling cascade. We found that mTORC1 targets, mTOR, 4EBP1, S6K, and S6, were most potently and consistently inhibited by ONC212 in U87 and NCH644 stem-like GBM cells (Fig. 2A; Supplementary Fig. S2A).

To determine if the potency of imipridones correlates with the regulation of apoptosis mediators (Bcl-2 family proteins; ref. 13), including their chaperones, Usp9X and Bag3, we assessed as to whether or not ONC201 derivatives, ONC206 and ONC212, would regulate the protein levels of those molecules in a more potent manner. We found that in U87 and stem-like GBM cells, NCH644, ONC206 and ONC212 at 200 nmol/L suppressed the expression levels of antiapoptotic, Bcl-2, Bcl-xL and Mcl-1, and the deubiquitinase Usp9X, whereas in contrast at the same concentration, ONC201 was less effective (Fig. 2B; Supplementary Fig. S2B). Under these conditions, proapoptotic Bcl-2 family members, BIM and Noxa, were downregulated after ONC206 and ONC212 treatment (Fig. 2B; Supplementary Fig. S2B). However, ONC201 (10 μ mol/L) upregulated BIM in U87 cells, priming cells for potential proapoptotic stimuli (Fig. 2B; Supplementary Fig. S2B). In essence, these findings support the idea that imipridones convert the cells into a more "apoptosis favorable" state.

Imipridones downregulate protein levels of the transcription factor, c-myc, at the posttranslational level

We found substantial evidence for suppression of c-myc downstream targets by imipridones in accordance with their potency (Fig. 2C). We conducted a time course experiment to assess c-myc protein levels and detected a downregulation of c-myc as early as 2 hours and extending to 72 hours after imipridone treatment in established and stem-like GBM cells (Fig. 2D and H). Of note, ONC212 had the strongest impact on c-myc levels, consistent with its strongest potency among imipridones. We hypothesized that based on our transcriptome analysis, most likely imipridones modulate the stability of c-myc protein because this transcription factor is known to have a very short half-life and is highly susceptible to proteasomal degradation upon phosphorylation at threonine 58. Therefore, we conducted a time course analysis of phosphorylated and total c-myc protein levels upon stimulation with imipridones (Fig. 2H). Although ONC201 led to a rapid depletion of total c-myc protein (within 2 hours) and decrease of phosphorylated c-myc at serine 62, it increased phosphorylation of c-myc at threonine 58, which was preceded and coincided with a reduction in phosphorylation of GSK3 β at serine 9, a kinase that is known to phosphorylate c-myc at threonine 58 (Fig. 2H; refs. 23, 24). Given that GSK3 β is a substrate of AKT, we assessed AKT phosphorylation status and found that ONC201 decreased phosphorylation of AKT at serine 473, coinciding with GSK3 β

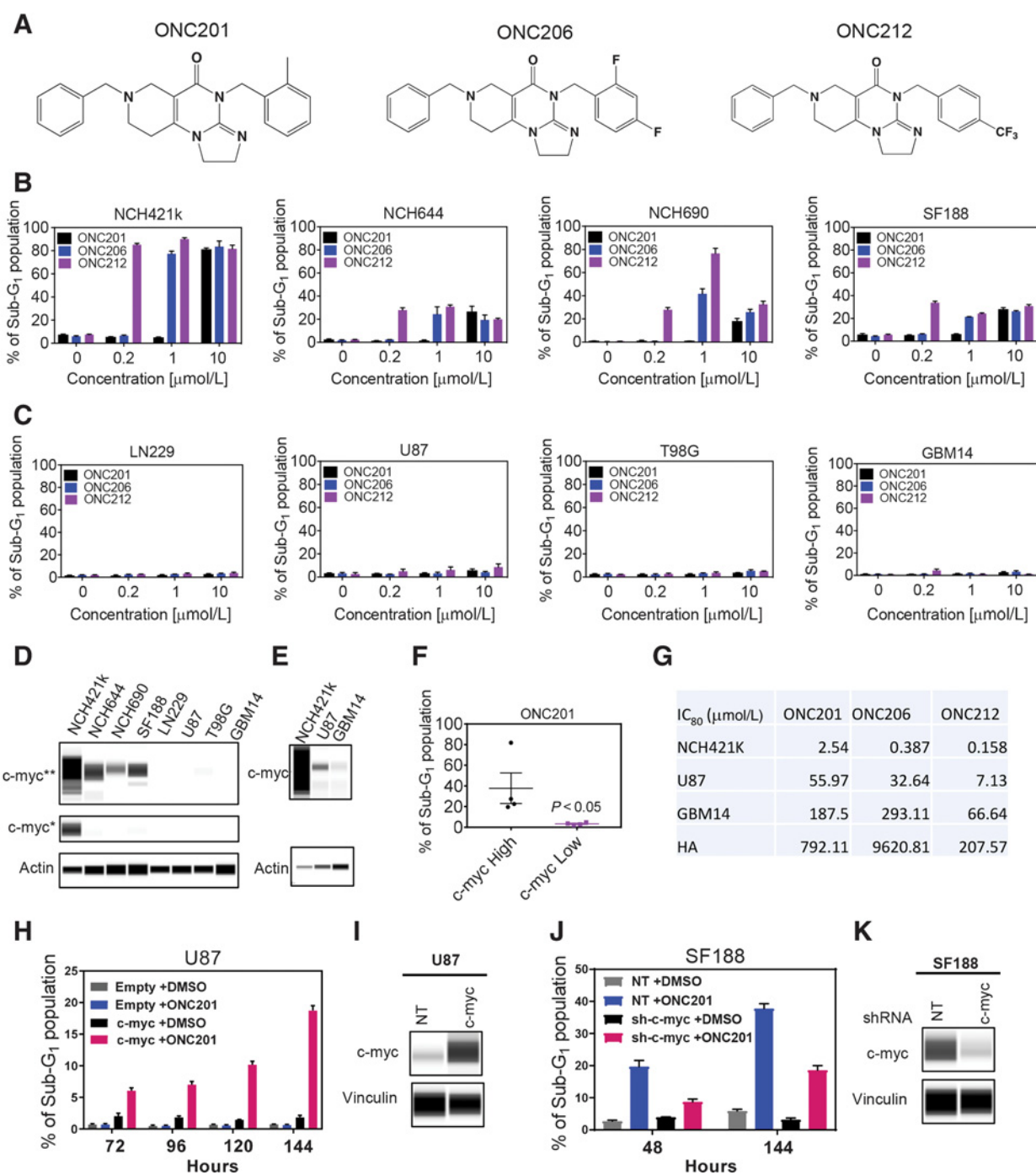
dephosphorylation (Fig. 2H). Consistently, two pharmacologic inhibitors of GSK3 β restored c-myc protein levels upon imipridone treatment (Fig. 2I), confirming the pivotal role of GSK3 β in imipridone-mediated reduction of c-myc protein levels. Moreover, imipridones did not suppress protein levels of a T58A c-myc mutant (a hotspot region for mutations), further supporting the role of GSK3 β in the mechanism (Fig. 2J). To confirm that these phosphorylation events of c-myc result in a decrease of c-myc stability, U87 GBM cells were treated with ONC212 or DMSO and exposed to protein synthesis inhibitor, cycloheximide. ONC212 reduced the stability of c-myc protein (Fig. 2E and 2F). Next, we treated U87 GBM cells with ONC212 in the presence or absence of the bona fide proteasomal inhibitor, MG132. In keeping with the initial hypothesis, MG132 attenuated ONC212-mediated suppression of c-myc protein (Fig. 2G). Similar findings were made with the lead compound ONC201 (Supplementary Fig. S2D and S2E). To determine the relative contribution of c-myc mRNA suppression by imipridones, we treated U87GBM cells with various concentration of ONC201, ONC206, and ONC212 and assessed c-myc mRNA levels. We found only slight suppression of c-myc mRNA levels, suggesting that the major effect of imipridones on c-myc is nontranscriptional (Supplementary Fig. S3A and S3B). Overall, these findings suggest that imipridone enhances c-myc degradation, most likely through regulation of the proteasomal pathway, involving GSK3 β -mediated phosphorylation of threonine 58.

Next, we posed the question as to whether or not simultaneous targeting of c-myc along with imipridones provides a potential therapeutic benefit. To this end, we utilized a bromodomain protein inhibitor (BRD2-4), OTX015, a compound that has been shown to transcriptionally antagonize the expression of c-myc (25, 26), and tested the efficacy of imipridones in the presence or absence of this inhibitor in stem-like GBM cells, NCH644 and NCH421k. NCH644 and NCH421k cells were treated with OTX015, imipridones, or the combination and analyzed for apoptosis by Annexin V/PI staining with subsequent flow cytometry. In the presence of OTX015, imipridone-induced apoptosis was significantly enhanced (Supplementary Fig. S2C), suggesting that dual-targeting c-myc by BRD4 inhibitors and imipridones might be viable treatment strategy that is effective against tumor-initiating cells.

Imipridones reprogram the transcriptome of GBM cells and suppress glycolysis and oxidative phosphorylation

In order to identify the underlying mechanisms by which imipridones elicit their antiglioma effects, we conducted a transcriptome analysis and subsequent GSEA of GBM cells treated with ONC201, ONC206, and ONC212 (at 200 nmol/L) as well as ONC201 at 10 μ mol/L. In keeping with the Western blot findings, we only identified transcriptomic changes in cells treated with ONC206 and ONC212 at 200 nmol/L, whereas ONC201 appeared to elicit no effects at that concentration (not shown). However, higher concentrations of ONC201 (10 μ mol/L) resembled the effects of ONC206 and ONC212. Our GSEA uncovered additional mechanistic insights into the biology of imipridones. Most notably, we found changes related to cellular metabolism that suggest that imipridones suppress glycolysis as well as oxidative phosphorylation, resulting in a "transcriptional state of energy starvation" (Fig. 3A). These findings were linked to changes in the expression of relevant associated transcription factors. As mentioned earlier, we identified several gene sets to be

Ishida et al.

**Figure 1.**

Imipridones cause inhibition of cellular proliferation in a range of model systems of glioblastoma, including PDX, stem-like and established GBM cells, and induce apoptosis in a c-myc protein expression level-dependent manner. **A**, Chemical structures of the imipridones used in the current study. The lead compound is ONC201, whereas ONC206 and ONC212 are chemical derivatives. **B**, High c-myc-expressing GBM cultures, NCH421k (stem-like GBM cells), NCH644, NCH690, and pediatric SF188 GBM cells were treated with increasing concentrations of ONC201, ONC206, and ONC212 for 72 hours, fixed, stained with propidium iodide, and analyzed by flow cytometry. Shown are mean percentages with SD of cells in the sub-G₁ fraction. **C**, Low c-myc-expressing established GBM cells, LN229, U87, and T98G, and PDX cells, GBM14, were treated with increasing concentrations of ONC201, ONC206, and ONC212 for 72 hours were fixed, stained with propidium iodide, and analyzed by flow cytometry. Shown are mean percentages with SD of cells in the sub-G₁ fraction. **D**, GBM stem-like cells, NCH421k, NCH644, and NCH690, and established GBM cells, SF188 (c-myc amplified, pediatric GBM), LN229, U87, T98G, and GBM14 (PDX GBM cells) were analyzed by capillary electrophoresis for the protein expression levels of c-myc and Actin. Two stars (**) and one star (*) indicate long and short exposure times, respectively. **E**, High (NCH421k), intermediate (U87), and low (GBM14) cells were analyzed for the expression of c-myc. **D** to **E** constitute same samples with different exposures. (Continued on the following page.)

downregulated related to c-myc targets (Supplementary Fig. S3A), suggesting that first c-myc is likely a key player in imipridone-mediated anti glioma activity and that second c-myc is likely responsible for the transcriptional metabolic reprogramming of GBM cells by imipridones because many of the c-myc targets are genes implicated in metabolism.

In light of these transcriptional findings, we hypothesized that imipridones affect ATP levels of tumor cells. Our results suggest that ONC201 and ONC206 reduce ATP levels in a dose-dependent manner (Fig. 3B). Notably, ONC212 was most efficacious to reduce ATP levels, followed by ONC206 and ONC201 (Fig. 3B). Accompanied by the decline of ATP levels, we found an increase of phosphorylation of the AMP-sensitive kinase, AMPK (threonine 172), starting as early as 24 hours (Supplementary Fig. S3C). In keeping with the ATP levels, ONC212 was most potent in enhancing the phosphorylation of AMPK. It is generally accepted that low energy levels are causal for the accumulation of unfolded proteins in the endoplasmic reticulum. In keeping with that notion, we found evidence of activation of several ER stress-related pathways as manifested by elevation of IRE1 α , ATF4, ATF3, and phosphorylated eif2 α proteins (Supplementary Fig. S3D).

Because the global transcriptome analysis suggests an inhibition of glycolysis and oxidative energy metabolism (Supplementary Fig. S4A–S4E), we conducted extracellular flux analysis. To this purpose, SF188 (high c-myc) and U87 (intermediate c-myc levels) GBM cells were treated with vehicle, ONC201, ONC206, or ONC212 and assayed for glycolytic activity by extracellular flux analysis (Fig. 3C–E; Supplementary Figs. S4E–S4L and S5A–S5E). We found that imipridones, ONC206 and ONC212, were most potent to suppress baseline extracellular acidification rate (ECAR; Supplementary Fig. S5A–S5E), which was more pronounced in high c-myc-expressing SF188 cells as compared with U87 (Fig. 3E). However, utilizing 10 μ mol/L of the lead compound, ONC201, recapitulated the effects of ONC206 and ONC212 on glycolysis (Supplementary Fig. S4F–S4I). In addition, we tested whether or not c-myc-overexpressing U87 cells are more susceptible to glycolysis inhibition by imipridones. As shown in Fig. 3F, c-myc-overexpressing cells are more susceptible to ECAR reduction as compared with vector-transduced cells. We assessed the protein levels of glycolysis-related enzymes and transporters, HK2, LDHA, and GLUT1. To this purpose, U87 cells were treated with various imipridones as above. We found that ONC206 and ONC212 reduced the levels of HK2, GLUT1, and LDH (Fig. 3G). In order to confirm that imipridone-mediated suppression of c-myc is sufficient to affect glycolysis, we performed knockdown experiments, involving two c-myc siRNA oligonucleotides. There was an siRNA-dependent reduction in c-myc protein levels and an associated depletion of HK2, LDHA, and GLUT1, in keeping with the hypothesis that c-myc governs the expression of these proteins and that this is also true in the setting of GBM model systems (Fig. 3). To further delineate the role of c-myc in glycolytic

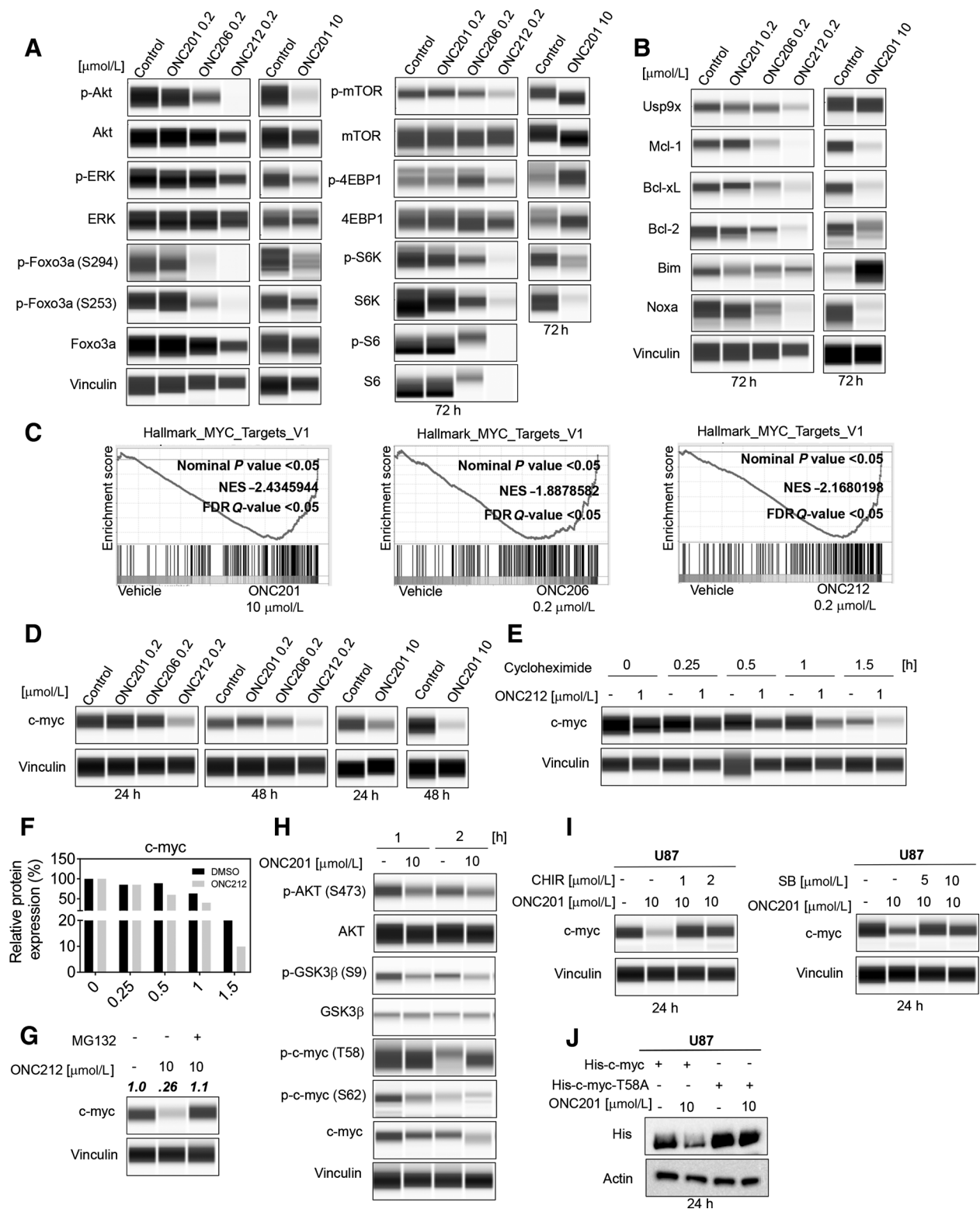
metabolism, we pharmacologically inhibited c-myc by using OTX015. We have previously shown that the concentrations of OTX015 applied in the current studies were sufficient to suppress c-myc protein levels (10, 27). Using this dosage of OTX015, we performed extracellular flux analysis. We found that c-myc inhibition recapitulates the effects on ECAR-mediated imipridones, furthermore suggesting the pivotal role of c-myc in imipridone-mediated glycolytic inhibition (Fig. 3I). To further assess the impact of imipridones on glycolysis, we measured glycolytic metabolites by LC/MS following ONC212 treatment. These results show that ONC212 leads to an accumulation of glycolytic metabolites, suggesting a glycolytic block with an overall reduction of glycolysis (as supported by the extracellular flux analysis with reduction in ECAR; Fig. 3J).

Next, we determined the effects of imipridones on OXPHOS-related metabolism. To this end, U87 GBM cells were treated with vehicle, ONC201, ONC206, and ONC212 for 24 hours and analyzed for basal oxygen consumption rate (OCR), ATP production, and maximal respiration (Fig. 4A–C; Supplementary Fig. S5F). We detected a significant reduction in all these parameters in cells treated with 200 nmol/L ONC206 and ONC212 (Fig. 4A–C; Supplementary Fig. S5F). In contrast, 200 nmol/L of ONC201 had little effect on mitochondrial respiration (Fig. 4A and B). However, 10 μ mol/L of ONC201 recapitulated the effects of ONC206 on ONC212 (Fig. 4A–C; Supplementary Fig. S5H), further corroborating the earlier notion that ONC206 and ONC212 are more potent than ONC201. We assessed the relative potency of imipridone OCR reduction in the context of high and intermediate c-myc expression. As anticipated, high c-myc-expressing SF188 cells were more prone to OCR inhibition by imipridones as compared with U87 cells (Fig. 4C).

Given the significant suppression of OXPHOS, we evaluated the underlying mechanisms governing these changes. We conducted Western blot analysis to detect the expression levels for respiratory complexes, pyruvate dehydrogenase (PDH). To this purpose, U87, LN229, and stem-like GBM cells, NCH644, were treated with vehicle, ONC201, ONC206, and ONC212 for 72 hours (Fig. 4D; Supplementary Fig. S5H and S5I). Although no effects on the expression of respiratory complexes were detected with 200 nmol/L of ONC201, the imipridone derivatives, ONC206 and ONC212, suppressed the levels of OXPHOS complexes as well as of PDH at that concentration (Fig. 4D). However, 10 μ mol/L of ONC201 suppressed OXPHOS complexes as well (Fig. 4D; Supplementary Fig. S5H and S5I). Similarly, c-myc knockdown also affected the protein expression of respiratory complexes (Fig. 4E and F), in keeping with the effects of imipridones. To assess the functional implication of c-myc on OXPHOS in glioblastoma cells, U87 GBM cells were treated with OTX015 for 24 hours and subsequently analyzed by extracellular flux analysis. OTX-015 reduced the OCR (Fig. 4G). Given the suppression of OXPHOS, we analyzed TCA metabolite levels upon

(Continued.) **F**, Cell cultures analyzed in **E** were treated with ONC201 at 10 μ mol/L for 72 hours and analyzed for the percentage of apoptotic cells by flow cytometry (data extrapolated from the analysis in **B** and **C**). Cells were then grouped in accordance with their c-myc levels (high: NCH421k, NCH644, NCH690, and SF188; intermediate to low: LN229, U87, T98G, and GBM14). Shown are mean values with SD ($P < 0.05$). **G**, Cells from **E** (high c-myc: NCH421k, intermediate c-myc: U87, and low c-myc: GBM14) as well as nonneoplastic human astrocytes were treated with increasing concentrations of imipridones. Nonlinear regression was used to calculate the IC₅₀ values. **H** and **I**, U87 GBM cells were transduced with a control (empty) or human c-myc encoding lentivirus and selected by puromycin. Enhanced expression of c-myc was verified by capillary electrophoresis (**I**). Control- and c-myc-overexpressing U87 cells were treated with 10 μ mol/L ONC201, fixed and stained with propidium iodide, and analyzed for DNA fragmentation by flow cytometry. **J** and **K**, SF188 (pediatric glioblastoma with MYC amplified) were transduced with lentiviral particles, containing either a nontargeting (NT) or human c-myc targeting shRNA. Cells were selected with puromycin to obtain stable cultures. Silencing of c-myc was confirmed by capillary electrophoresis (**K**). Nontargeting and c-myc shRNA-containing cells were treated with 10 μ mol/L ONC201 for the indicated time frame, fixed, stained with propidium iodide, and analyzed for DNA fragmentation. Shown are mean with SD.

Ishida et al.

**Figure 2.**

Imipridones suppress protein levels of the transcription factor, c-myc, through modulation of its stability via GSK3 β . **A** and **B**, U87 were treated with the indicated imipridones derivatives. After the indicated time points, whole-cell protein lysates were prepared and subjected to capillary electrophoresis, using the Wes instrument (Proteinsimple). **C**, U87 GBM cells were treated with DMSO or ONC201, ONC206, or ONC212 at the indicated concentrations for 72 hours. Thereafter, RNA was isolated, subjected to microarray analysis, and followed by GSEA. (Continued on the following page.)

treatment with imipridone derivatives by LC/MS. In keeping with the findings obtained with the extracellular flux analysis, we encountered a suppression of TCA cycle intermediates (Fig. 4H), further corroborating the earlier notion that imipridones significantly impair tumor energy metabolism. Consistent with an impact on mitochondrial metabolism, we found a significant suppression of mtDNA levels in imipridone-treated U87 GBM cells, which is most pronounced in ONC212-treated cells (Fig. 4I). Similarly, mitochondrial membrane potential was lowered by ONC212 (Supplementary Fig. S5G).

Imipridones enhance serine-one carbon-glycine metabolism

Although imipridones suppress the main energetic metabolic pathways of GBM cells, we were hypothesizing that compensatory pathways will be activated. In this vein, GSEA provided information that imipridone-treated GBM cells activate the serine-one carbon-glycine metabolism with an increase of *PHGDH*, *PSAT1*, and *PSPH* and other enzyme-related genes to the folate cycle (Fig. 5A; Supplementary Fig. S6A). These findings were confirmed by real-time PCR and protein expression analysis in both glioblastoma and colonic carcinoma cells, suggesting that these observations are not limited to just GBM (Fig. 5B and D; Supplementary Fig. S7A). Consistently, we found that depriving GBM cells of energy (ATP) by the ATP synthase inhibitor, oligomycin, upregulates *PHGDH* and *PSAT1*, in keeping with our hypothesis that energy deprivation leads to the activation of this pathway (Supplementary Fig. S6D). To corroborate these findings, LC/MS analysis was performed, which showed significant increases of metabolites related to the serine-one carbon-glycine metabolism in imipridone-treated cells (Fig. 5C). To address the question by which mechanism imipridones induce this pathway, we consulted our GSEA data and the literature and concluded that likely ATF4 is the pivotal mediator of these transcriptional changes. To test this hypothesis, we silenced ATF4 levels in the presence or absence of imipridones and found that ATF4 silencing (involving one siRNA pool, four distinct siRNAs, and a shRNA construct) attenuates imipridone-mediated increase of *PHGDH* and *PSAT1* (Fig. 5E; Supplementary Figs. S6B and S6C, and S7B and S7C). Next, we determined the translational impact of pharmacologic targeting of the SOG pathway along with imipridones. To this end, we used two recently identified pharmacologic inhibitors of *PHGDH*, NCT-503, and CBR-5884 (28), and combined them with ONC212. We found that the combination treatment of NCT-503 and ONC212 enhanced induction of apoptosis more potent than each compound alone in stem-cell like GBM cells, NCH421k, NCH644, and NCH690, as well as in U87 GBM cells (Fig. 5F). Similar results were obtained when we administered CBR-5884 in lieu of NCT-503 (Fig. 5G). These synergistic apoptotic effects were not limited to glioblastoma model systems since HCT116 colon carcinoma cells showed a comparable

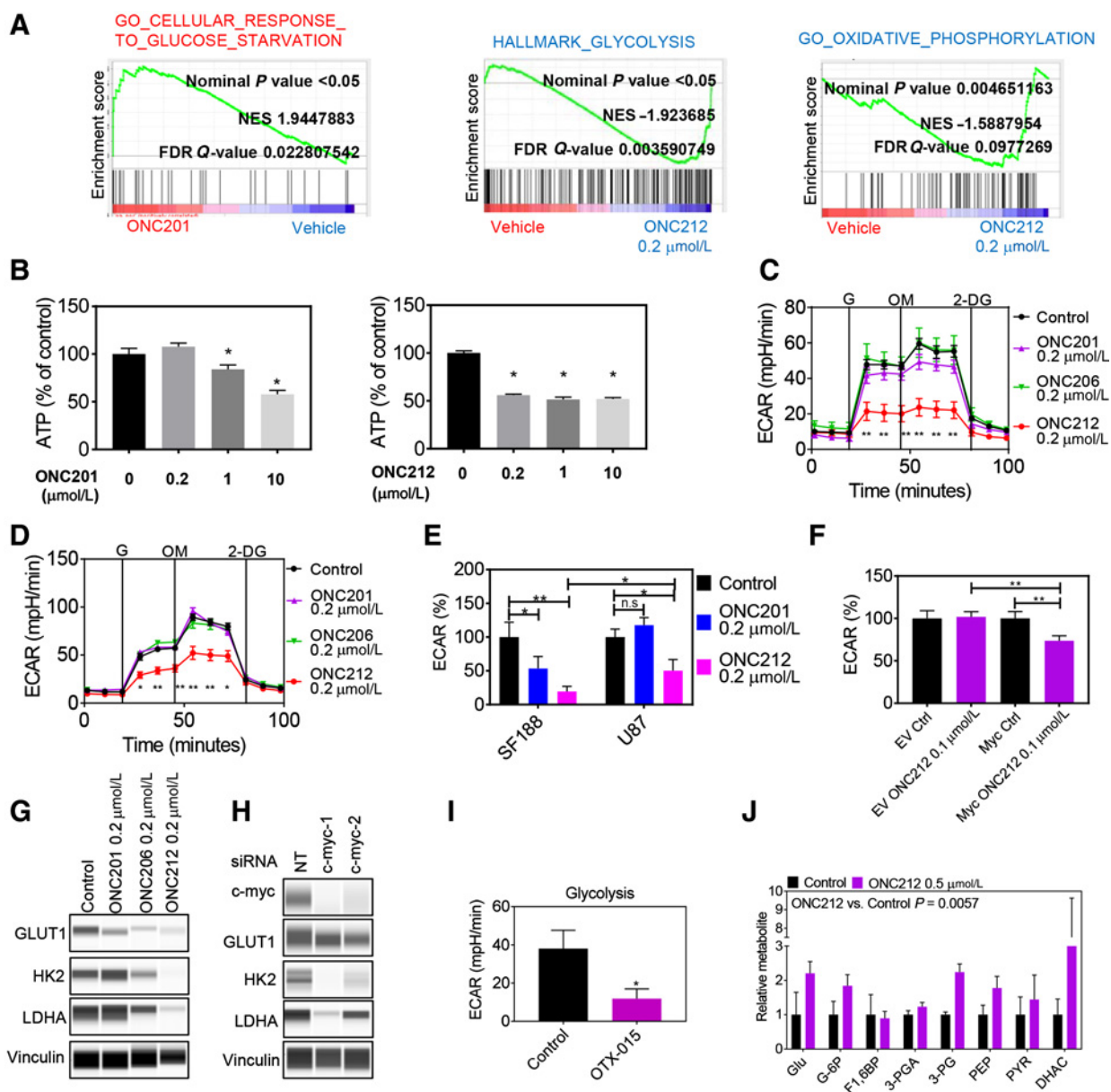
response rate to the combination treatment (Supplementary Fig. S7D). The findings of the activation of the SOG pathway are summarized in Supplementary Fig. S7G.

The novel imipridone derivatives are active either singly or in combination therapies in multiple xenograft models and extend host survival in orthotopic PDXs of GBMs

PDX model systems remain the most relevant preclinical model systems to predict antitumor responses in patients, which is accepted in the studies of GBM as well. Following this strategy, we compared the efficacy of the lead compound, ONC201, with the chemical derivative, ONC212, which was the most potent in all assays related to *in vitro* testing. To this purpose, we used two PDX models, GBM12 and GBM43, that have different mutational backgrounds and susceptibilities to the standard-of-care treatment (temozolomide; ref. 29). These lines were implanted in immunocompromised mice, and after tumors were established, three treatment groups were formed, consisting of vehicle, ONC201, and ONC212. Treatment was performed 2 times a week. Unanimously, we found that ONC212 was most potent in reducing tumor growth (Supplementary Fig. S8A–S8F), intimating that imipridones are efficacious in relevant preclinical animal models of GBM and that chemical modification results in an improvement of efficacy of imipridones. Finally, to account for all here studied imipridones, we conducted a third animal model, using the highly challenging to treat U87-EGFRvIII model. Tumor cells were implanted subcutaneously, and upon establishment of the tumors, three groups were formed for subsequent treatments with vehicle, ONC206, and ONC212. Upon conclusion of the study, host tumor sizes in animals treated with ONC212 were the smallest as compared with vehicle or ONC206 (Supplementary Fig. S8G–S8I), in keeping with the results in the PDX models. To account for toxicity, we measured the weights of the animals and found no significant weight loss by imipridone derivatives (Supplementary Fig. S8I). With respect to morphologic appearance, we noted that tumors treated with imipridones were smaller, and on the histopathologic level, ONC212 showed the most prominent reduction in cellular density and mitotic rate and an increase in cell death (Supplementary Fig. S9C and S9E). We assessed the effects on imipridones on cellular proliferation *in vivo* by staining for Ki67. In comparison with vehicle, both ONC201 and ONC212 reduced the proliferation index and number of positive cells (Supplementary Fig. S9C). However, ONC212 was most potent. To assess the amount of apoptosis induced by imipridones *in vivo*, we stained tumor section for TUNEL. Although vehicle and ONC201 revealed minimal staining, ONC212 displayed significantly more positive tumor cells (Supplementary Fig. S9D). These observations are in keeping with the significantly smaller tumor size in animals that were

(Continued.) Shown is the gene set for MYC-related transcriptional targets. NES, Normalized enriched score. **D**, U87 GBM cells were treated with the indicated imipridones. Whole-cell protein lysates were harvested and analyzed by capillary electrophoresis for c-myc and Vinculin. **E**, U87 GBM cells were pretreated with ONC212. Thereafter, cells were exposed to cycloheximide for the indicated time points. Whole-protein lysates were collected and analyzed for the expression of c-myc by capillary electrophoresis. **F**, Quantification for the analysis as shown in **E**. Shown are mean of relative percentages compared with either vehicle- or ONC212-treated samples (time point 0 hour). **G**, U87 GBM cells were treated with ONC212 in the presence or absence of MG132. Whole-protein lysates were collected and analyzed by capillary electrophoresis. **H**, U87 GBM cells were treated as indicated, and whole-protein lysates were prepared. Lysates were subjected to capillary electrophoresis on the Wes simple instrument (Proteinsimple). Shown are protein levels of phosphorylated Akt (Serine 473), total Akt, phosphorylated GSK3 β (Serine 9), total GSK3 β , phosphorylated c-myc (Threonine 58), total c-myc, and Vinculin. **I**, U87 GBM cells were treated in the presence or absence of GSK3 β inhibitors, CHIR-908014 or SB216763. Whole-cell protein lysates were harvested and analyzed for the expression of c-myc and Vinculin. **J**, U87 GBM cells were transfected with a plasmid for c-myc wild-type or c-myc T58A mutant (both containing a His-tag). Thereafter, GBM cells were treated with vehicle or ONC201 at the indicated concentration. Whole-cell protein lysates were collected and subjected to standard Western blotting analysis. Shown are the expression levels for His and Actin.

Ishida et al.

**Figure 3.**

Imipridones, ONC201, ONC206, and ONC212, suppress glycolytic energy metabolism. **A**, U87 GBM cells were treated with ONC201 or ONC212 for 72 hours. Thereafter, RNA was analyzed, and subsequently whole-transcriptome analysis was performed by microarray analysis, followed by GSEA. Shown are plots for glucose starvation (upregulated), glycolysis (downregulated), and oxidative phosphorylation (downregulated). NES, normalized enrichment score. **B**, U87 GBM cells were treated with ONC201 and ONC212 for 24 hours and analyzed for ATP content. Shown are mean values with SD. $n = 3$ biological replicates. * indicates a $P < 0.05$ between control and treatment. **C** and **D**, SF188 (**C**) and U87 (**D**) GBM cells were treated with the indicated compounds for 24 hours. Thereafter, extracellular flux analysis for ECAR was performed in the context of a glycolytic stress assay. Shown are ECAR values. Shown are mean with SEM. G, Glucose; OM, Oligomycin; 2-DG, 2-deoxyglucose. **E**, Comparison between ECAR values in SF188 (high c-myc) and U87 GBM (intermediate c-myc) cells. **F**, Empty vector or c-myc-transduced U87 cells were treated with ONC212 and analyzed for ECAR. Shown are percentages relative to the controls. **G**, U87 GBM cells were treated with the respective imipridones as indicated for 72 hours and analyzed for the expression of glycolytic transporters (GLUT1) and enzymes (LDHA, HK2). **H**, GBM cells were transfected with two different siRNA oligonucleotides, targeting c-myc, or with nontargeting siRNA. Seventy-two hours after transfection, whole-protein lysates were prepared and analyzed by capillary electrophoresis for glycolytic transporters (GLUT1) and enzymes (HK2, LDHA) as well as for c-myc expression. **I**, U87 GBM cells were treated with 5 $\mu\text{mol/L}$ OTX-015 (an inhibitor of BRD proteins). Cells were analyzed by extracellular flux analysis in the context of a glycolytic stress assay. Shown are mean and SD. ** means P value less than 0.01, whereas * indicates P of less than 0.05. **J**, U87 GBM cells were treated with vehicle or ONC212. Thereafter, cells were harvested for LC/MS analysis for the indicated glycolytic or pentose phosphate pathway-related metabolites. Glu, Glucose; G-6P, Glucose-6-phosphate; F1,6BP, Fructose-1,6-bisphosphate; 3-PGA, Glyceraldehyde-3-phosphate; 3-PG, 3-Phosphoglycerate; PEP, Phosphoenolpyruvate; Pyr, Pyruvate; DHAC, Dihydroxyacetonephosphate; 6-PG, 6-Phosphogluconate; RR-5-P, Ribose-ribulose-5-phosphate.

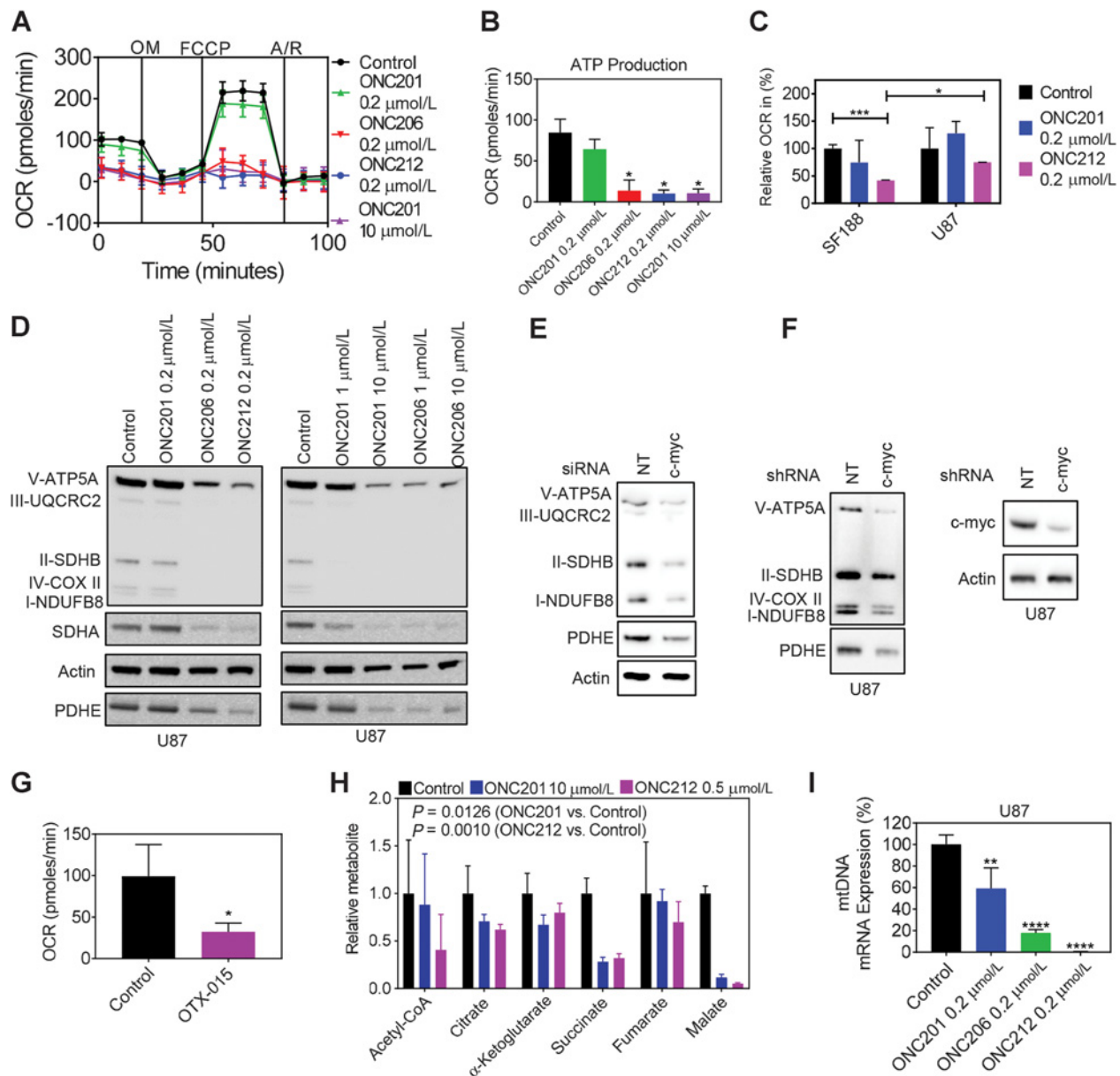
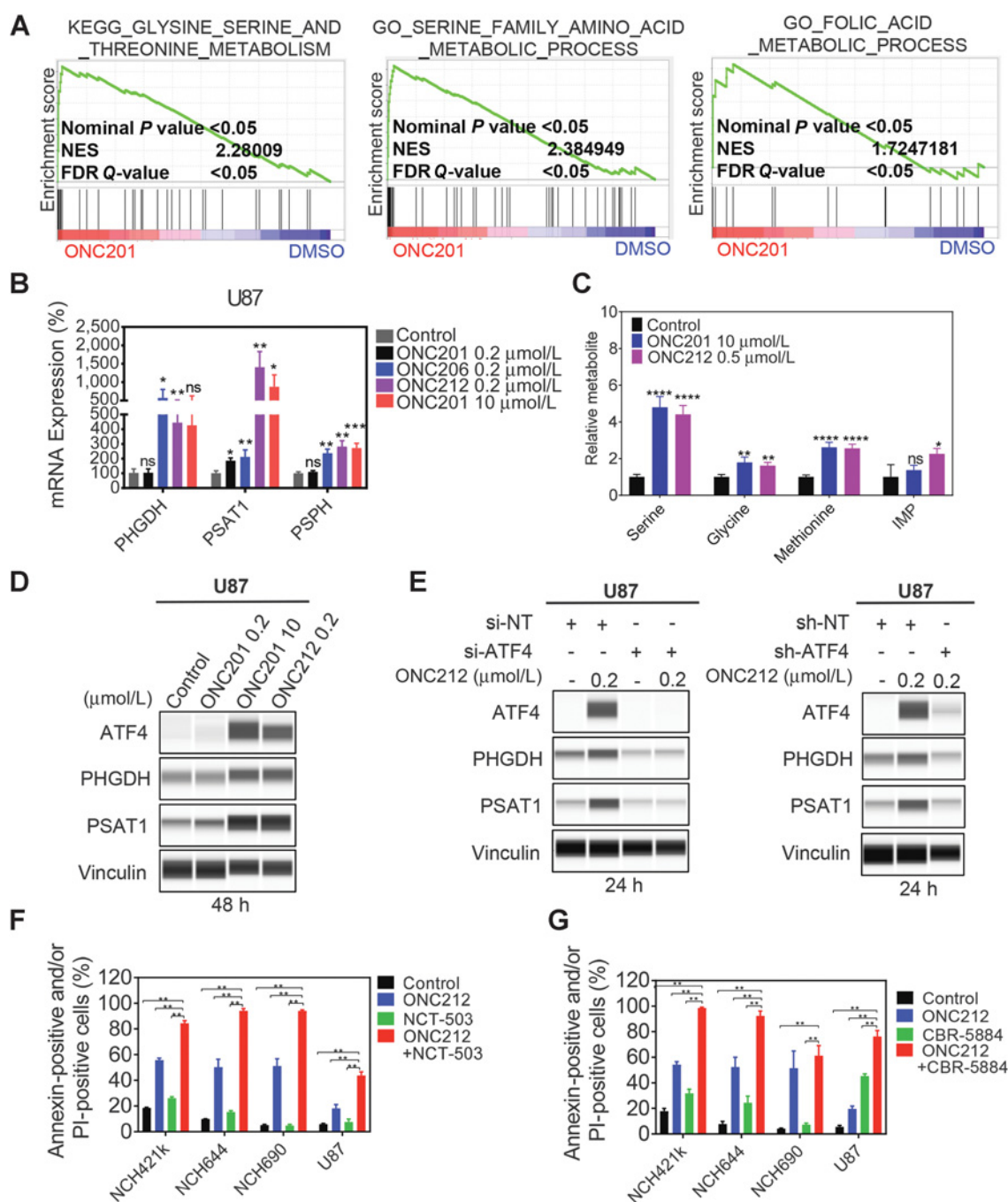


Figure 4. Imipridones inhibit oxidative phosphorylation and reduce the expression of respiratory complexes, metabolites of the TCA cycle, and mitochondrial biogenesis. **A** and **B**, U87 GBM cells were treated as indicated for 24 hours and analyzed for extracellular flux (Seahorse XFe24). Shown are mitochondrial respiration (mitochondrial OCR) and OXPHOS-related ATP production. Shown are mean and SD. **C**, SF188 and U87 GBM cells were treated as indicated and subjected to assessment of the OCR. Shown are percentages relative to control. **D**, U87 GBM cells were treated as indicated for 72 hours. Whole-cell protein lysates were collected and analyzed by conventional Western blotting. Shown are the expression of the five respiratory complexes and PDH. **E**, GBM cells were transfected with one siRNA oligonucleotide, targeting c-myc, or with non-targeting siRNA. 72 h after transfection, whole protein lysates were prepared and analyzed for the expression of respiratory complexes and PDH (conventional Western blotting). **F**, U87 GBM cells were transfected with nontargeting or MYC-specific shRNA lentiviral particles. Stable c-myc and nontargeting shRNA-expressing cells were selected. Thereafter, whole-cell protein lysates were prepared and analyzed for the expression of respiratory complexes and PDH (conventional Western blotting). **G**, U87 GBM cells were treated as indicated for 24 hours and subjected to extracellular flux analysis. OCR was determined. Shown are mean with SD. **H**, U87 GBM cells were treated with vehicle, ONC212, or ONC201. Thereafter, cells were harvested for LC/MS analysis for metabolites related to the TCA cycle. **I**, U87 GBM cells were treated with imipridone derivatives as indicated, RNA was harvested, and cDNA was analyzed for mtDNA levels relative to nuclear levels. Shown are mean with SD. ** means P value less than 0.01, whereas * indicates P of less than 0.05.

treated with ONC212. Taken together, these results intimate that imipridone derivatives are potential drug compounds for the treatment of malignant glial brain tumors.

Based on these results, we extended our studies to orthotopic PDXs of glioblastoma with high or low c-myc expression (Supplementary Fig. S8J) in order to test the hypothesis that high levels

Ishida et al.

**Figure 5.**

Imipridones activate the serine-one carbon-glycine pathway, and interference with this pathway sensitizes for imipridone-mediated apoptosis *in vitro* and *in vivo*. **A**, U87 GBM cells were treated with DMSO or ONC201, ONC206 or ONC212 at the indicated concentrations for 72 hours. Thereafter, RNA was isolated, subjected to microarray analysis, followed by GSEA. Shown is the gene set for serine-one carbon-glycine-related transcriptional targets. NES, Normalized enriched score. **B**, U87 GBM cells were treated as indicated. RNA was harvested, reverse transcribed, and cDNA was amplified for PHGDH, PSAT1, and PSPH. Shown are mean and SD. **C**, U87 GBM cells were treated with imipridones. Lysates were processed for LC/MS and analyzed for the indicated metabolites related to serine-one carbon-glycine metabolism. IMP, inosine monophosphate. **D**, U87 GBM cells were treated with the indicated imipridones. Whole-cell protein lysates were prepared and analyzed for expression of the indicated proteins. **E**, U87 GBM cells were transfected with nontargeting siRNA or ATF4-specific siRNA. Thereafter, cells were treated with the indicated imipridone. Whole-cell protein lysates were harvested and analyzed for the indicated proteins by capillary electrophoresis. U87 cells were transfected with nontargeting shRNA or ATF4-specific lentiviral particles. Stable cell lines were generated, plated, and treated with ONC212. Whole-cell protein lysates were collected and analyzed for the expression of the indicated proteins (right). **F** and **G**, GBM stem cells, NCH421k, NCH644, and NCH690, and established GBM cells, U87, were treated with imipridones in the presence or absence of PHGDH inhibitor, NCT-503, or CBR-5884 for 96 hours. Thereafter, cells were labeled with Annexin V/propidium iodide and analyzed by flow cytometry. Shown are mean and SD. **/***/**** means P value less than 0.01, whereas * indicates P of less than 0.05.

of c-myc protein predict a better response to imipridone treatment in the most preclinical relevant models. GBM123 cells (high c-myc protein) were more susceptible to imipridones as compared with U87 GBM cells (low-to-intermediate c-myc protein levels; Supplementary Fig. S8J–S8L). For these experiments, we used the most potent imipridone, ONC212, given the well-known challenges of treating orthotopic glioblastoma models. U87 or GBM123 cells were injected into the brain of nude mice. After establishment of tumors, animals were treated with vehicle or ONC212. Although in the U87 model we only detected a small survival benefit, we found a substantial increase of overall survival in the ONC212 treatment group in the GBM123 model (Fig. 6A and B). Notably, when comparing the survival curves of ONC212 in both the U87 and GBM123 model, we found that ONC212 prolonged host survival significantly longer as compared with the U87 model, suggesting that high c-myc protein levels predict a longer host survival upon imipridone treatment ($P < 0.05$).

Given the role of c-myc in imipridone-mediated cell death, the *in vivo* implication of high c-myc levels, and our earlier findings that interference with c-myc by BRD4 inhibitors enhances the efficacy of imipridones, we assessed the combination treatment strategy of imipridones and BRD4 inhibitors in a xenograft model, utilizing the NCH644, stem-like GBM cells. Although single treated host animals revealed a slight reduction in tumor growth, the combined treatment of ONC201 along with OTX015 led to a significant reduction in tumor growth with significant cell death/necrosis (Fig. 6C–F). Despite this efficacy, the combination treatment had no effect on the viability of organs, such as brain, heart, lung, liver, intestine, spleen, and kidney, and did not induce significant weight loss (Supplementary Fig. S9A and S9B). Finally, we confirmed that PHGDH inhibitors and imipridones reduce tumor growth synergistically *in vivo*. To this purpose, we tested the glioblastoma model system, U87-EGFRvIII. Host animals treated with the combination treatment of ONC212 and NCT-503 had significantly smaller tumors than single or vehicle treatments (Fig. 6G). As an additional model system, the HCT116 colon carcinoma xenograft model was tested. In like manner, host animals that received the combination treatment of ONC212 and NCT-503 had significantly smaller tumors than single or vehicle treatments (Fig. 6H–I; Supplementary Fig. S7E and S7F).

Discussion

Glioblastoma remains one of the biggest challenges in medicine, and thus far, researchers have not been successful to provide a substantial improvement in prognosis for this detrimental disease (30). Despite the fact that alike other tumors GBMs have known recurrent genetic alterations and certain point mutations for which an arsenal of inhibitors already exists, none of these compounds has shown a durable response clinically (31, 32). The reason for these failures might be multiple, but certainly related to the fact that GBMs have a substantial, intrinsic heterogeneity that in itself requires either pleiotropic drug compounds that interfere with multiple pathways or a rational drug combination therapy at the onset (27, 33–38).

Imipridone derivatives elegantly fit into this category because these compounds act on several pivotal pathways for gliomagenesis, maintenance, and progression of these neoplasms, e.g., AKT and ERK signaling and the antiapoptotic Bcl-2 family members of proteins (13). The first compound out of this category is TIC10/ONC201 that was discovered in an attempt to identify com-

pounds that increase expression for the death ligand TRAIL (3). Shortly thereafter, it was suggested that ONC201 elicits the induction of an integrated stress response, involving the transcription factor, ATF4 (4), leading to an inhibition of proliferation of cancer cells. However, the underlying mechanism as to how this happens remained elusive, and our current study provides significant additional novel insight about the underlying events.

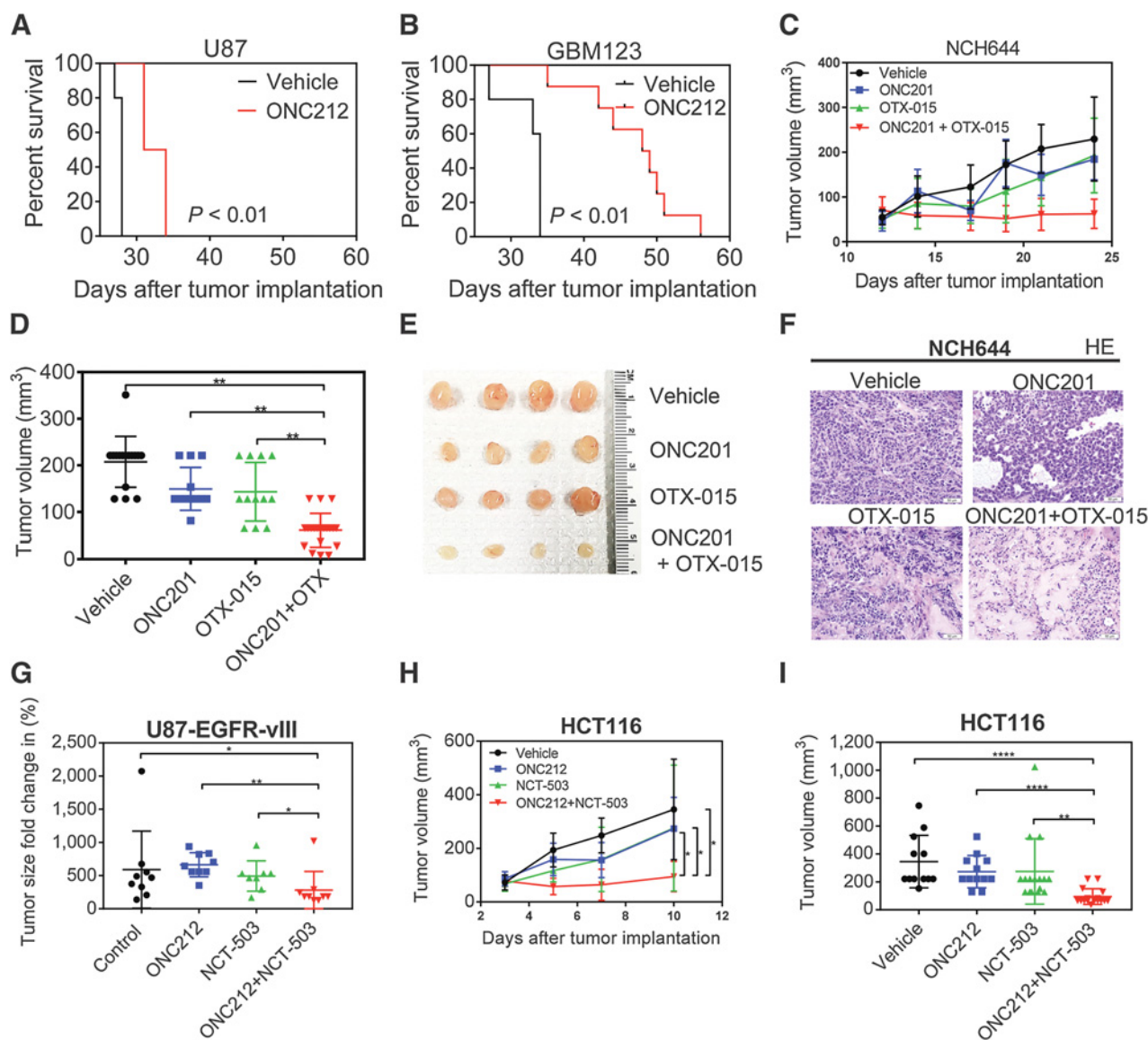
Having discovered a potent class of molecules with anticancer properties, it was tempting to develop derivatives that are more potent than the lead compound. Examples of this strategy are the imipridones, ONC206 and ONC212 (2). In our studies, we found that ONC212 was the most potent inhibitor with respect to antiangioma activity, followed by ONC206 and ONC201. These results are in keeping with one earlier study that focused on pancreatic adenocarcinoma model systems (2).

In seeking more upstream mechanisms as to how imipridones elicit their antiangioma activity, we conducted transcriptome analysis with subsequent GSEA and metabolite analysis by LC/MS. We made the novel observation that imipridones affected energy metabolism by suppression of genes encoding for enzymes and metabolites related to glycolysis and oxidative phosphorylation. Consistently, the proteins related to those genes were down-regulated as well. To the best of our knowledge, these findings have not been reported thus far and mechanistically significantly extend the understanding of how imipridones elicit their antitumor effects. Given that many tumors are "glycolytic" in nature, it is a notable finding that imipridones interfere with both OXPHOS and glycolysis because many compounds that target only one of these pathways, such as 2-DG, will result in the compensatory activation of other major metabolic energy pathways. For instance, 2-DG inhibits glycolysis, and in turn, tumor cells activate oxidative phosphorylation to balance their energy needs. Mechanistically, this is owed in part due to mitochondrial plasticity as 2-DG inhibits mitochondrial fission, leading to enhanced fusion by modulation of the phosphorylation status of Drp1 (39). Our findings also show that imipridones regulate mitochondrial plasticity because they lead to enhanced mitochondrial fission, which in turn dampens OXPHOS activity. Another example is gemcitabine resistance in model systems of pancreatic cancer because these tumors enhance glucose metabolism to escape from therapy (40). In this context, it may be tempting to speculate as to whether or not imipridones might reverse gemcitabine resistance or act synergistically to reduce tumor cell proliferation with this chemotherapeutic drug.

To compensate for this massive impact on tumor cell energy metabolism by imipridones, we found that these compounds activate the serine-one carbon-glycine pathway that is utilized by several types of tumors to support growth. Interestingly, the literature also suggests a role for this pathway to synthesize ATP independent of OXPHOS and glycolysis (41). Therefore, imipridone might utilize this pathway in part to produce energy. In keeping with its prosurvival function (42–45), interference with this pathway through PHGDH inhibition (28), using two novel pharmaceutical inhibitors, leads to synergistic cell death *in vitro* and *in vivo*. Although we have not evaluated methotrexate in combination with imipridone, it is likely that this compound might synergize with imipridones as well because methotrexate interferes with the folate cycle and thus with the serine-glycine pathway.

We determined the mechanism how imipridones suspend energy metabolism in tumor cells and found that the transcription

Ishida et al.

**Figure 6.**

Imipridones extend host survival in PDX models of GBM and reduce tumor growth synergistically with BRD4 and PHGDH inhibitors. **A**, U87 GBM cells (low-to-intermediate *c-myc* levels) were implanted intracranially in nude mice. After randomization in two groups, treatment was initiated with either vehicle or ONC212 (100 mg/kg) twice a week. Primary endpoint for these experiments is survival or a moribund state of the animal. Shown are Kaplan–Meier survival curves, and the log-rank test was applied to calculate statistical significance. **B**, PDX cells, GBM123 (high *c-myc*-expressing tumors), were implanted intracranially in nude mice. After randomization in two groups, treatment was initiated with either vehicle or ONC212 (100 mg/kg) twice a week. Primary endpoint for these experiments is survival or a moribund state of the animal. Shown are Kaplan–Meier survival curves, and the log-rank test was applied to calculate statistical significance. **C–E**, Stem-like GBM cells, NCH644, were implanted subcutaneously. Once tumors were established, animals were randomized into four designated groups, vehicle, ONC201 (100 mg/kg), OTX015 (OTX; 75 mg/kg), or the combination of ONC201+OTX015. Treatments were given 3 times a week. Caliper measurements were performed, and tumor volumes were calculated as previously described. At the end of the experiment, statistical analysis is performed, using the Mann–Whitney test. A *P* value of less than 0.05 was considered statistically significant. Shown are scatter plots with mean and SD. Gross images of the explanted tumors are provided in **E**. **F**, Representative histologic images of the individual treatments of the xenografts performed in **C**. Slides were stained with hematoxylin and eosin (HE). **G**, U87-EGFR-vIII cells were implanted subcutaneously in nude mice. After establishment of tumors, four groups were formed as indicated: Vehicle, ONC212 (50 mg/kg), NCT-503 (50 mg/kg), or the combination of ONC212 and NCT-503. Shown are scatter plots of relative tumor fold changes (%) with mean and SD (last day of experiment; normalization is to 100% at the start of the experiment). **H**, HCT116 cells were implanted subcutaneously in nude mice. After establishment of tumors, four groups were formed as indicated: Vehicle, ONC212 (50 mg/kg), NCT-503 (50 mg/kg), or the combination of ONC212 and NCT-503. Shown are mean and SD. **I**, Scatter plots of the final tumor sizes on the day of conclusion of the experiment. ** means *P* value less than 0.01, whereas * indicates *P* of less than 0.05.

factor c-myc (46–48) is involved in this process. Although c-myc was not downregulated at the level of transcription, we found a marked decrease of c-myc on the protein level as early as 1 hour after treatment. Consistently, cells with high levels of c-myc are more susceptible to imipridone treatment, an important finding that has not been shown previously before. Given that GBM stem-like cells are known to be highly dependent on c-myc, our observation that imipridones induce massive apoptosis in these cells is in keeping with this earlier notion. Therefore, our findings suggest that imipridones have the potential to eradicate the stem-cell fraction within a glial neoplasm, thus counteracting the development of treatment resistance and recurrence. Similarly, the pediatric GBM cell line SF188 (c-myc amplified) displays high sensitivity to imipridone derivative, suggesting that c-myc status may predict apoptotic susceptibility to imipridone derivatives. However, it should be noted that even tumor cells with lower expression levels of c-myc display an antiproliferative response to imipridones, albeit without significant apoptosis induction. Our findings also demonstrate that inhibition of c-myc superenhancers by BRD4 inhibitors along with imipridones synergistically reduces the viability of glioma cells *in vitro* and *in vivo*, which has not been shown in other tumor entities before. Therefore, it might be tempting to speculate whether or not nonsolid malignancies might respond to this novel combination therapy as well.

Finally, we confirmed whether or not imipridones prolong host survival in orthotopic xenograft models. Our findings showed that ONC212 extended host survival in a high c-myc-expressing PDX model, whereas in a low c-myc-expressing model system, these antiglioma effects were significantly less pronounced. These findings support the overall notion that high c-myc levels predict therapeutic responses to imipridones and that chemical modification of imipridones potentially enhances antitumor activity.

Taken together, these findings provide a foundation for clinical testing of these compounds either singly or in combination regimes in patients. In addition, utilization of c-myc as a biomarker might be a strategy for prediction of therapeutic responses.

References

- Allen JE, Krigsfeld G, Mayes PA, Patel L, Dicker DT, Patel AS, et al. Dual inactivation of Akt and ERK by TIC10 signals Foxo3a nuclear translocation, TRAIL gene induction, and potent antitumor effects. *Sci Transl Med* 2013;5:171ra17.
- Wagner J, Kline CL, Ralff MD, Lev A, Lulla A, Zhou L, et al. Preclinical evaluation of the imipridone family, analogs of clinical stage anti-cancer small molecule ONC201, reveals potent anti-cancer effects of ONC212. *Cell Cycle* 2017;16:1790–9.
- Allen JE, Prabhu VV, Talekar M, van den Heuvel AP, Lim B, Dicker DT, et al. Genetic and pharmacological screens converge in identifying FLIP, BCL2, and IAP proteins as key regulators of sensitivity to the TRAIL-inducing anticancer agent ONC201/TIC10. *Cancer Res* 2015;75:1668–74.
- Kline CL, Van den Heuvel AP, Allen JE, Prabhu VV, Dicker DT, El-Deiry WS. ONC201 kills solid tumor cells by triggering an integrated stress response dependent on ATF4 activation by specific eIF2alpha kinases. *Sci Signal* 2016;9:ra18.
- Prabhu VV, Allen JE, Dicker DT, El-Deiry WS. Small-molecule ONC201/TIC10 targets chemotherapy-resistant colorectal cancer stem-like cells in an Akt/Foxo3a/TRAIL-dependent manner. *Cancer Res* 2015;75:1423–32.
- Kline CLB, Ralff MD, Lulla AR, Wagner JM, Abbosh PH, Dicker DT, et al. Role of dopamine receptors in the anticancer activity of ONC201. *Neoplasia* 2018;20:80–91.
- Willems L, Jacque N, Jacquel A, Neveux N, Maciel TT, Lambert M, et al. Inhibiting glutamine uptake represents an attractive new strategy for treating acute myeloid leukemia. *Blood* 2013;122:3521–32.
- Qing G, Li B, Vu A, Skuli N, Walton ZE, Liu X, et al. ATF4 regulates MYC-mediated neuroblastoma cell death upon glutamine deprivation. *Cancer Cell* 2012;22:631–44.
- Dranoff G, Elion GB, Friedman HS, Bigner DD. Combination chemotherapy *in vitro* exploiting glutamine metabolism of human glioma and medulloblastoma. *Cancer Res* 1985;45:4082–6.
- Ishida CT, Shu C, Halatsch ME, Westhoff MA, Altieri DC, Karpel-Massler G, et al. Mitochondrial matrix chaperone and c-myc inhibition causes enhanced lethality in glioblastoma. *Oncotarget* 2017;8:37140–53.
- Wang J, Wang H, Li Z, Wu Q, Lathia JD, McLendon RE, et al. c-Myc is required for maintenance of glioma cancer stem cells. *PLoS One* 2008;3:e3769.
- Filippakopoulos P, Qi J, Picaud S, Shen Y, Smith WB, Fedorov O, et al. Selective inhibition of BET bromodomains. *Nature* 2010;468:1067–73.
- Karpel-Massler G, Ba M, Shu C, Halatsch ME, Westhoff MA, Bruce JN, et al. TIC10/ONC201 synergizes with Bcl-2/Bcl-xL inhibition in glioblastoma by suppression of Mcl-1 and its binding partners *in vitro* and *in vivo*. *Oncotarget* 2015;6:36456–71.
- Karpel-Massler G, Kast RE, Westhoff MA, Dwucet A, Welscher N, Nonnenmacher L, et al. Olanzapine inhibits proliferation, migration and anchorage-independent growth in human glioblastoma cell lines and enhances temozolomide's antiproliferative effect. *J Neurooncol* 2015;122:21–33.
- Karpel-Massler G, Shu C, Chau L, Banu M, Halatsch ME, Westhoff MA, et al. Combined inhibition of Bcl-2/Bcl-xL and Usp9X/Bag3 overcomes

Disclosure of Potential Conflicts of Interest

V.V. Prabhu is an employee of and holds ownership interest (including patents) in Oncocotics. J.E. Allen holds ownership interest (including patents) in Oncocotics. No potential conflicts of interest were disclosed by the other authors.

Authors' Contributions

Conception and design: C.T. Ishida, Y. Zhang, V.V. Prabhu, J.E. Allen, M.D. Siegelin

Development of methodology: C.T. Ishida, G. Karpel-Massler, V.V. Prabhu, M.D. Siegelin

Acquisition of data (provided animals, acquired and managed patients, provided facilities, etc.): C.T. Ishida, Y. Zhang, C. Shu, G. Kleiner, M.J. Sanchez-Quintero, M.D. Siegelin

Analysis and interpretation of data (e.g., statistical analysis, biostatistics, computational analysis): C.T. Ishida, Y. Zhang, M.D. Siegelin

Writing, review, and/or revision of the manuscript: C.T. Ishida, Y. Zhang, E. Bianchetti, C.M. Quinzii, M.-A. Westhoff, G. Karpel-Massler, V.V. Prabhu, J.E. Allen, M.D. Siegelin

Administrative, technical, or material support (i.e., reporting or organizing data, constructing databases): E. Bianchetti, C. Shu, T.T.T. Nguyen, V.V. Prabhu, M.D. Siegelin

Study supervision: C.M. Quinzii, M.D. Siegelin

Acknowledgments

This work was supported by the NIH NINDS K08NS083732, R01NS095848, R01NS102366, the 2017 American Brain Tumor Association Discovery Grant (DG1700013), and Louis V. Gerstner, Jr. Scholars Program (2017-2020). The flow cytometry experiments were performed in the CCI Flow Cytometry Core, supported in part by the Office of the Director, NIH under award S10RR027050. Transcriptome analysis was supported by the CTSA grant UL1-TR001430 to the Boston University Microarray and Sequencing Resource Core Facility.

The costs of publication of this article were defrayed in part by the payment of page charges. This article must therefore be hereby marked *advertisement* in accordance with 18 U.S.C. Section 1734 solely to indicate this fact.

Received April 3, 2018; revised June 16, 2018; accepted July 17, 2018; published first July 23, 2018.

- apoptotic resistance in glioblastoma in vitro and in vivo. *Oncotarget* 2015;6:14507–21.
16. Karpel-Massler G, Ishida CT, Bianchetti E, Shu C, Perez-Lorenzo R, Horst B, et al. Inhibition of mitochondrial matrix chaperones and antiapoptotic Bcl-2 family proteins empower antitumor therapeutic responses. *Cancer Res* 2017;77:3513–26.
 17. Karpel-Massler G, Pareja F, Aime P, Shu C, Chau L, Westhoff MA, et al. PARP inhibition restores extrinsic apoptotic sensitivity in glioblastoma. *PLoS One* 2014;9:e114583.
 18. Sheng Z, Li L, Zhu LJ, Smith TW, Demers A, Ross AH, et al. A genome-wide RNA interference screen reveals an essential CREB3L2-ATF5-MCL1 survival pathway in malignant glioma with therapeutic implications. *Nat Med* 2010;16:671–7.
 19. Tang M, Gao G, Rueda CB, Yu H, Thibodeaux DN, Awano T, et al. Brain microvasculature defects and Glut1 deficiency syndrome averted by early repletion of the glucose transporter-1 protein. *Nat Commun* 2017;8:14152.
 20. Gui DY, Sullivan LB, Luengo A, Hosios AM, Bush LN, Gitego N, et al. Environment dictates dependence on mitochondrial complex I for NAD⁺ and aspartate production and determines cancer cell sensitivity to metformin. *Cell Metab* 2016;24:716–27.
 21. Karpel-Massler G, Ishida CT, Bianchetti E, Zhang Y, Shu C, Tsujiuchi T, et al. Induction of synthetic lethality in IDH1-mutated gliomas through inhibition of Bcl-xL. *Nat Commun* 2017;8:1067.
 22. Siegelin MD, Dohi T, Raskett CM, Orlowski GM, Powers CM, Gilbert CA, et al. Exploiting the mitochondrial unfolded protein response for cancer therapy in mice and human cells. *J Clin Invest* 2011;121:1349–60.
 23. Welcker M, Orian A, Jin J, Grim JE, Harper JW, Eisenman RN, et al. The Fbw7 tumor suppressor regulates glycogen synthase kinase 3 phosphorylation-dependent c-Myc protein degradation. *PNAS* 2004;101:9085–90.
 24. Wang X, Cunningham M, Zhang X, Tokarz S, Laraway B, Troxell M, et al. Phosphorylation regulates c-Myc's oncogenic activity in the mammary gland. *Cancer Res* 2011;71:925–36.
 25. Berenguer-Daize C, Astorgues-Xerri L, Odore E, Cayol M, Cvitkovic E, Noel K, et al. OTX015 (MK-8628), a novel BET inhibitor, displays in vitro and in vivo antitumor effects alone and in combination with conventional therapies in glioblastoma models. *Int J Cancer* 2016;139:2047–55.
 26. Amorim S, Stathis A, Gleeson M, Iyengar S, Magarotto V, Leleu X, et al. Bromodomain inhibitor OTX015 in patients with lymphoma or multiple myeloma: a dose-escalation, open-label, pharmacokinetic, phase 1 study. *Lancet Haematol* 2016;3:e196–204.
 27. Ishida CT, Bianchetti E, Shu C, Halatsch ME, Westhoff MA, Karpel-Massler G, et al. BH3-mimetics and BET-inhibitors elicit enhanced lethality in malignant glioma. *Oncotarget* 2017;8:29558–73.
 28. Pacold ME, Brimacombe KR, Chan SH, Rohde JM, Lewis CA, Swier LJ, et al. A PHGDH inhibitor reveals coordination of serine synthesis and one-carbon unit fate. *Nat Chem Biol* 2016;12:452–8.
 29. Gupta SK, Kizilbash SH, Carlson BL, Mladek AC, Boakye-Agyeman F, Bakken KK, et al. Delineation of MGMT hypermethylation as a biomarker for veliparib-mediated temozolomide-sensitizing therapy of glioblastoma. *J Natl Cancer Inst* 2015;108.
 30. Hegi ME, Diserens AC, Gorlia T, Hamou MF, de Tribolet N, Weller M, et al. MGMT gene silencing and benefit from temozolomide in glioblastoma. *N Engl J Med* 2005;352:997–1003.
 31. Siegelin MD. Inhibition of the mitochondrial Hsp90 chaperone network: a novel, efficient treatment strategy for cancer? *Cancer Lett* 2013;333:133–46.
 32. Siegelin MD. Utilization of the cellular stress response to sensitize cancer cells to TRAIL-mediated apoptosis. *Expert Opin Ther Targets* 2012;16:801–17.
 33. Pareja F, Macleod D, Shu C, Cray JF, Canoll PD, Ross AH, et al. PI3K and Bcl-2 inhibition primes glioblastoma cells to apoptosis through downregulation of Mcl-1 and Phospho-BAD. *Mol Cancer Res* 2014;12:987–1001.
 34. Karpel-Massler G, Ramani D, Shu C, Halatsch ME, Westhoff MA, Bruce JN, et al. Metabolic reprogramming of glioblastoma cells by L-asparaginase sensitizes for apoptosis in vitro and in vivo. *Oncotarget* 2016;7:33512–28.
 35. Karpel-Massler G, Horst BA, Shu C, Chau L, Tsujiuchi T, Bruce JN, et al. A synthetic cell-penetrating dominant-negative ATF5 peptide exerts anticancer activity against a broad spectrum of treatment-resistant cancers. *Clin Cancer Res* 2016;22:4698–711.
 36. Karpel-Massler G, Banu MA, Shu C, Halatsch ME, Westhoff MA, Bruce JN, et al. Inhibition of deubiquitinases primes glioblastoma cells to apoptosis in vitro and in vivo. *Oncotarget* 2016;7:12791–805.
 37. Ghosh JC, Siegelin MD, Vaira V, Favarsani A, Tavecchio M, Chae YC, et al. Adaptive mitochondrial reprogramming and resistance to PI3K therapy. *J Natl Cancer Inst* 2015;107.
 38. Karpel-Massler G, Ishida CT, Zhang Y, Halatsch ME, Westhoff MA, Siegelin MD. Targeting intrinsic apoptosis and other forms of cell death by BH3-mimetics in glioblastoma. *Expert Opin Drug Discov* 2017;12:1031–40.
 39. Li J, Huang Q, Long X, Guo X, Sun X, Jin X, et al. Mitochondrial elongation-mediated glucose metabolism reprogramming is essential for tumour cell survival during energy stress. *Oncogene* 2017;36:4901–12.
 40. Shukla SK, Purohit V, Mehla K, Gunda V, Chaika NV, Vernucci E, et al. MUC1 and HIF-1alpha signaling crosstalk induces anabolic glucose metabolism to impart gemcitabine resistance to pancreatic cancer. *Cancer Cell* 2017;32:71–87e7.
 41. Tedeschi PM, Markert EK, Gounder M, Lin H, Dvorzhinski D, Dolfi SC, et al. Contribution of serine, folate and glycine metabolism to the ATP, NADPH and purine requirements of cancer cells. *Cell Death Dis* 2013;4:e877.
 42. Zhang B, Zheng A, Hydbring P, Ambrose G, Ouchida AT, Goiny M, et al. PHGDH defines a metabolic subtype in lung adenocarcinomas with poor prognosis. *Cell Rep* 2017;19:2289–303.
 43. DeNicola GM, Chen PH, Mullarky E, Sudderth JA, Hu Z, Wu D, et al. NRF2 regulates serine biosynthesis in non-small cell lung cancer. *Nat Genet* 2015;47:1475–81.
 44. Possemato R, Marks KM, Shaul YD, Pacold ME, Kim D, Birsoy K, et al. Functional genomics reveal that the serine synthesis pathway is essential in breast cancer. *Nature* 2011;476:346–50.
 45. Locasale JW, Grassian AR, Melman T, Lyssiotis CA, Mattaini KR, Bass AJ, et al. Phosphoglycerate dehydrogenase diverts glycolytic flux and contributes to oncogenesis. *Nat Genet* 2011;43:869–74.
 46. Xiao ZD, Han L, Lee H, Zhuang L, Zhang Y, Baddour J, et al. Energy stress-induced lncRNA FILNC1 represses c-Myc-mediated energy metabolism and inhibits renal tumor development. *Nat Commun* 2017;8:783.
 47. Fang X, Zhou W, Wu Q, Huang Z, Shi Y, Yang K, et al. Deubiquitinase USP13 maintains glioblastoma stem cells by antagonizing FBXL14-mediated Myc ubiquitination. *J Exp Med* 2017;214:245–67.
 48. Satoh K, Yachida S, Sugimoto M, Oshima M, Nakagawa T, Akamoto S, et al. Global metabolic reprogramming of colorectal cancer occurs at adenoma stage and is induced by MYC. *Proc Natl Acad Sci U S A* 2017;114:E7697–E706.

Clinical Cancer Research

Metabolic Reprogramming by Dual AKT/ERK Inhibition through Imipridones Elicits Unique Vulnerabilities in Glioblastoma

Chiaki T. Ishida, Yiru Zhang, Elena Bianchetti, et al.

Clin Cancer Res 2018;24:5392-5406. Published OnlineFirst July 23, 2018.

Updated version Access the most recent version of this article at:
[doi:10.1158/1078-0432.CCR-18-1040](https://doi.org/10.1158/1078-0432.CCR-18-1040)

Supplementary Material Access the most recent supplemental material at:
<http://clincancerres.aacrjournals.org/content/suppl/2018/07/21/1078-0432.CCR-18-1040.DC1>

Cited articles This article cites 46 articles, 13 of which you can access for free at:
<http://clincancerres.aacrjournals.org/content/24/21/5392.full#ref-list-1>

Citing articles This article has been cited by 1 HighWire-hosted articles. Access the articles at:
<http://clincancerres.aacrjournals.org/content/24/21/5392.full#related-urls>

E-mail alerts [Sign up to receive free email-alerts](#) related to this article or journal.

Reprints and Subscriptions To order reprints of this article or to subscribe to the journal, contact the AACR Publications Department at pubs@aacr.org.

Permissions To request permission to re-use all or part of this article, use this link
<http://clincancerres.aacrjournals.org/content/24/21/5392>.
Click on "Request Permissions" which will take you to the Copyright Clearance Center's (CCC) Rightslink site.